

A New Multiscale Computational Method for Mechanical Analysis of Closed Liquid Cell Materials

H.W. Zhang^{1,2}, J. Lv¹ and Y.G. Zheng¹

Abstract: A new multiscale computational method named as extended multiscale finite element method is proposed for the mechanical analysis of closed liquid cell materials. The numerical base functions for both the displacement field and the pressure of the incompressible fluid within the closed cells are employed to establish the relationship between the macroscopic deformation and the microscopic variables such as deformation, stress, strain and fluid pressure. The results show that the extended multiscale finite element method constructed with the conventional four-node quadrilateral coarse-grid elements sometimes will have strong boundary effects and cannot predict well the fluid pressure in the closed cells. Thus more reasonable higher order coarse-grid elements which can characterize more accurately the structural deformation of the closed cells are introduced. Furthermore, inspired by the periodic boundary conditions used in the homogenization method, the generalized periodic boundary conditions are proposed for the construction of the numerical base functions of the higher order elements. Numerical results indicate that the extended multiscale finite element method with higher order elements can be successfully used for the mechanical analysis of closed liquid cell materials. Particularly, combining with the periodic boundary conditions, the extended multiscale finite element method with higher order elements can give more accurate results.

Keywords: closed liquid cell materials, extended multiscale finite element method, higher order element, periodic boundary condition

1 Introduction

Over the past few years, there has been growing interest in the modeling of closed cell materials due to their important applications in material engineering, especially

¹ State Key Laboratory for Structural Analysis of Industrial Equipment, Department of Engineering Mechanics, Faculty of Vehicle Engineering and Mechanic, Dalian University of Technology, Dalian 116024, P R China

² Corresponding author. E_mail: zhanghw@dlut.edu.cn

in technology of fabrication of synthetic cellular materials, foam materials and intelligent materials, and in the mechanics of biological tissues. For instance, the closed liquid cell materials, which are common in roots, stems, and branches of plants, enable the plants to perform localized movement due to a biological process called nastic motion in specialized closed liquid cells. These cells can be considered as the muscles of biological systems and the driving units of the nastic motion. Inspired by the nastic movements, artificial nastic actuators, which allow for significant deformation through the mechanism of controlled charge and fluid across the cell membrane, have been utilized in the design of advanced actuators in recent years [Sundaresan and Leo (2005); Freeman and Weiland (2009); Piyasena, Newby, Miller, Shapiro and Smela, (2009)].

In the practical applications, due to the small scale of the component of the closed liquid cell materials, such as the biological membrane in nastic materials, these materials generally consist of a large number of microcapsules, as schematically shown in Fig. 1. The behavior of the closed liquid cell materials is influenced by the physical phenomena which take place on each scale and by the interaction of the phenomena across scales. In this context, even with the help of high-speed modern computers, the precise analysis of such kind of media with a large number of heterogeneities is extremely difficult for the standard finite element method (FEM). To overcome this difficulty, an effective way is to develop multiscale algorithms that are suitable for the numerical simulation of the closed liquid cell materials.

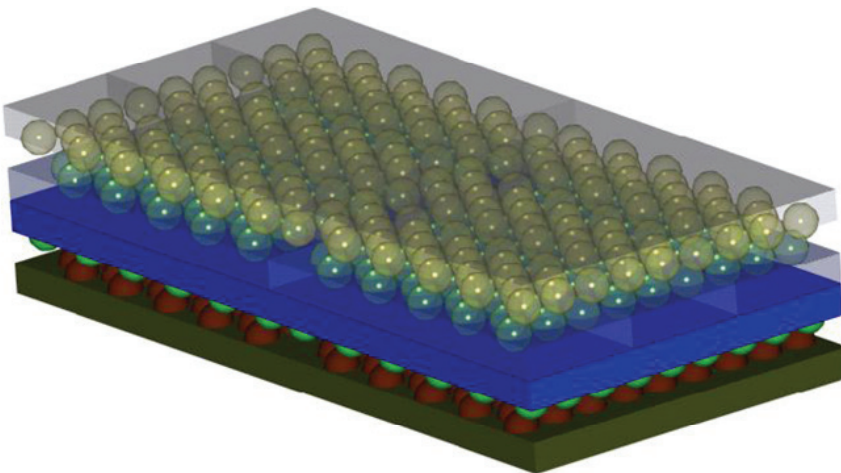


Figure 1: Structure diagram of nastic material for smart actuators [Sundaresan and Leo (2005)]

In recent years, a considerable number of multiscale methods have been developed and successfully applied to the heterogeneous problems [Schrefler, (2005); Yang and Becker (2004); Kanoute, Boso, Chaboche and Schrefler (2009)]. Notable among them are numerical homogenization methods, such as asymptotic computational homogenization method [Babuska, (1976); Benssousan, Lions and Papanicolaou (1978); Paumelle, Hassim and Lene (1991); Miehe and Bayreuther (2007), Yuan and Fish (2008)] and representative volume element (RVE) method [Suquet (1987); Okada, Fukui and Kumazawa (2004); Berger, Kari, Gabbert, Rodriguez-Ramos, Guinovart, Otero and Bravo-Castillero (2005); Wang and Yao (2005); Dang and Sankar (2008)]. In these methods, the FEM is applied to compute the homogenized material parameters as well as to evaluate the microscopic variables from the macroscopic response.

Despite their overall success, the numerical homogenization methods still have some challenges. Besides the local periodicity hypothesis, these methods request that the ratio between the small-scale length and the large-scale length is very small. These methods still require tremendous computational efforts in the downscaling computation and solving nonlinear problems [Fish, Shek, Pandheeradi and Shephard (1997); Terada and Kikuchi (2001); Zhang, Boso and Schrefler (2003)]. Moreover, the closed cells enclosing incompressible fluid make the problem much more difficult, requiring more extensive computational efforts by using the traditional homogenization methods.

The multiscale finite element method (MsFEM) can be traced back to the work presented by Babuska and Osborn (1983); Babuska, Caloz and Osborn (1994). It has been further extended by Hou and Wu (1997); Hou, Wu and Cai (1999) for numerically solving second order elliptic boundary value problems with high oscillating coefficients. The main idea of MsFEM is to construct the multiscale base functions (shape functions) that are adaptive to the local property of differential operator. The small-scale information is then brought to the large scale through the coupling of the global stiffness matrix, and the effect of the small scale on the large scale is effectively captured. The MsFEM has been generalized and successfully used for numerical simulation of two-phase flow in heterogeneous porous media [Hou (2005); Efendiev, Ginting, Hou and Ewing (2006); Aarnes (2006); Aarnes, Krogstad and Lie (2006)] and extended to solve nonlinear partial differential equations [Efendiev, Hou and Ginting (2004)]. At the same time, several other multiscale methods have also been developed, such as the multiscale finite volume method [Jenny, Lee and Tchelepi (2003)] and the finite volume multiscale finite element method [He and Ren (2005)]. Markovic and Ibrahimbegovic (2004) reported somewhat similar strategies of coupling meso (micro) and macro scales of material behaviors. In their work, the finite element method is used on both scales which

are strongly coupled. The coupling of the scales is obtained through the framework of localized Lagrangian multipliers.

A coupled multiscale finite element method was developed by Zhang, Fu and Wu (2009) for solving the coupling problems of consolidation of heterogeneous saturated porous media under external loading conditions. The extended multiscale finite element method (EMsFEM) was then developed by Zhang, Wu and Fu (2009) for the multiscale analysis of periodic lattice truss materials. In the EMsFEM, the coupled additional terms of base functions for the interpolation of the displacement field are introduced to consider the coupled effect among different directions in the multi-dimensional problems. Numerical tests show that the introduction of these terms significantly improves the accuracy of the multiscale method. In the spirit of the work [Zhang, Wu and Fu (2009)], the EMsFEM was successfully introduced to solve the elastic-plastic problems of periodic lattice truss materials [Zhang, Wu and Fu (2010)]. Furthermore, Zhang and his coworkers [Zhang, Wu, Lv and Fu (2010)] constructed the EMsFEM for solving the mechanical problems of heterogeneous continuum materials in elasticity. Their results show that the EMsFEM can execute the downscaling computation easily and the actual micro stress and strain within the unit cells can be obtained simultaneously in the multiscale computation. Thus, the EMsFEM has great potential for the strength analysis of heterogeneous materials.

The goal of this study is to develop an EMsFEM for the multiscale computation of the closed liquid cell materials. Different from the previous work, in the current approach, the incompressible feature of the fluid needs to be taken into account in the computational algorithm. Meanwhile, the distension and shrinkage processes of the cells need also to be treated. Thus, the concept of the pressure base functions is proposed to resolve the fluid pressure caused by the deformation of the structure. The effects of the volume expansion of the fluid in the closed cells of the structure are treated as the combination of the effects of the macroscopic equivalent forces on the full structure and the local response of the volume expansion on the unit cells. The macroscopic displacement field is solved under the macroscopic equivalent forces, and the local response is calculated on the fine-scale mesh of the unit cell under the volume expansion of the fluid. Based on these strategies, a good coincidence between the mechanical response of the closed cell structure obtained by the EMsFEM and the standard FEM is achieved. However, the numerical results also show that the EMsFEM constructed with the conventional four-node quadrilateral coarse-grid elements sometimes will induce strong boundary effects and cannot predict accurately the fluid pressure in the closed cells. Therefore, a more reasonable higher order coarse-grid element which can characterize more accurately the structural deformation of the closed liquid cell materials is proposed.

As pointed out by many researchers [Hou and Wu (1997); Efendiev, Hou and Gint-

ing (2004); Efendiev, Ginting, Hou and Ewing (2006); Zhang, Fu and Wu (2009); Zhang, Wu, and Fu (2009); Zhang, Wu, Liu and Fu (2010); Zhang, Wu, Lv and Fu (2010)], the boundary conditions for the construction of the numerical base functions of the MsFEM have big influence on capturing the small-scale information. As a consequence, by a judicious choice of appropriate boundary conditions, the accuracy of the EMsFEM can be significantly improved. Motivated by the periodic boundary conditions used in the conventional homogenization method, a novel approach for the construction of the numerical base functions of the unit cell is proposed by means of the periodic conditions [Zhang, Wu, Lv and Fu (2010)]. The results show that the periodic boundary conditions can give much improvement in accuracy compared with the linear boundary conditions and the oversampling technique developed in the early work. Therefore, in this paper, the periodic boundary conditions are introduced to construct the base functions of the closed liquid cell. Furthermore, the generalized periodic boundary conditions are developed to construct the numerical base functions of the higher order element. The numerical results indicate that the EMsFEM with the higher order elements can be successfully used to deal with the problems of the closed liquid cell materials. It could be also observed that the higher order elements with the periodic boundary conditions have more advantages than the conventional lower order elements.

The organization of the present paper is as follows. In Section 2, we briefly review the basic theories of the EMsFEM. In Section 3, the construction of the multiscale base functions for the closed liquid cell materials is presented. The equivalence technique of the volume expansion of the fluid in the closed cell is carried out in detail. Then a higher order coarse-grid element for the EMsFEM is introduced. In Section 4, we start out by introduce the periodic boundary conditions for the construction of the base functions of the closed liquid cell modeled by the conventional four-node quadrilateral elements. Then the generalized periodic boundary conditions for the higher order elements are introduced. The corresponding numerical results are presented in Section 5. Finally, some remarks are concluded.

2 Basic theories of the EMsFEM

2.1 Basic equations of the EMsFEM

In this section, we first briefly review the principal idea of the EMsFEM developed in [Zhang, Wu, Lv and Fu (2010)]. The EMsFEM is proposed for solving a class of vector field problems in solid mechanics which contain many spatial scales that are intractable using the direct methods. The central goal of the approach is to obtain the large-scale solutions on a coarse-scale mesh accurately and efficiently without resolving small-scale details. Its main idea is to incorporate the small-scale

information into numerical basis functions and capture their effects on the large scale via finite element computations. The ways to construct the base functions are the main differences between the standard FEM and the EMsFEM. For the standard FEM, the base functions are interpolation functions of the nodal point values of the elements. Thus, the parameters, such as elastic modulus, conductivity and permeability, should be constant in each element. On the other hand, the base functions of the EMsFEM are constructed numerically and can take into account the heterogeneities of the media in each coarse-grid element. Then, the finite element computation only needs to be handled on the coarse-scale mesh, which reduces the degrees of freedom of the computational model significantly.

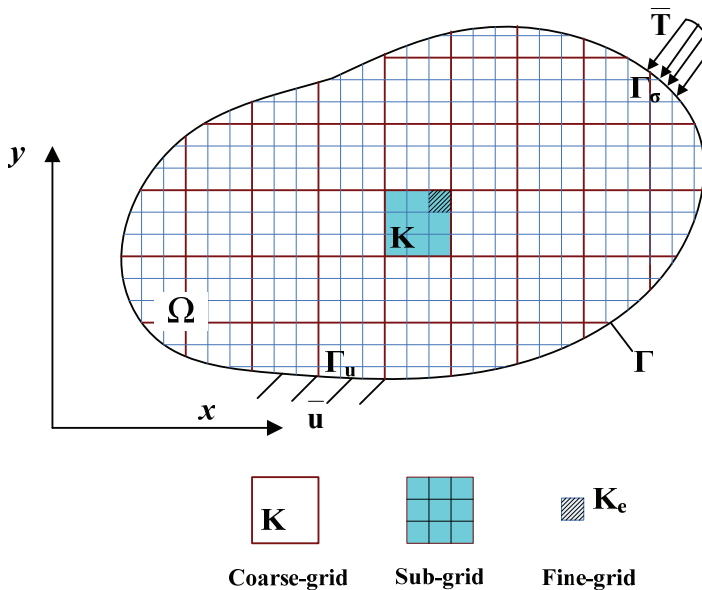


Figure 2: Schematic description of the EMsFEM

Let's consider a two-dimensional heterogeneous structure occupying a region Ω and having a boundary Γ as shown in Fig. 2. On part of the boundary Γ_σ , act traction $\bar{\mathbf{T}}$. Also, the boundary is constrained in region Γ_u , where displacements are specified as $\bar{\mathbf{u}}$. Then, the equilibrium equations and boundary conditions can

be expressed as

$$\begin{aligned}
 \operatorname{div}(\mathbf{D} : \mathbf{E}(\mathbf{u})) &= \bar{\mathbf{f}} \text{ in } \Omega \\
 \mathbf{n}\boldsymbol{\sigma} &= \bar{\mathbf{T}} \text{ on } \Gamma_{\sigma} \\
 \mathbf{u} &= \bar{\mathbf{u}} \text{ on } \Gamma_{\mathbf{u}}
 \end{aligned} \tag{1}$$

where \mathbf{D} is the fourth-order elasticity tensor representing material properties, $\mathbf{E}(\mathbf{u})$ is the strain tensor given as

$$\mathbf{E}(\mathbf{u}) = \frac{1}{2} \left(\nabla \mathbf{u} + (\nabla \mathbf{u})^T \right) \tag{2}$$

and \mathbf{u} is the displacement vector, $\boldsymbol{\sigma}$ is the stress vector which has three independent components, $\boldsymbol{\sigma} = [\sigma_x \quad \sigma_y \quad \tau_{xy}]^T$, $\bar{\mathbf{f}}$ is the body force vector, $\bar{\mathbf{f}} = [\bar{f}_x \quad \bar{f}_y]^T$, \mathbf{n} is the transformation matrix given as

$$\mathbf{n} = \begin{bmatrix} n_x & 0 & n_y \\ 0 & n_y & n_x \end{bmatrix} \tag{3}$$

There are two important computational steps which need to be implemented in the EMsFEM. One is a micro-scale computation in which the multiscale base functions of each coarse-grid element are constructed by solving local equilibrium equations on the sub-grid mesh (see Fig. 2) and then the equivalent stiffness matrices of the coarse-grid elements are derived. The other is the macro-scale computation. In this step, the FEM is handled on the coarse meshes since the coarse-grid elements' equivalent stiffness matrices have been obtained.

2.2 Micro-scale computation

2.2.1 The construction of the base functions

In the EMsFEM, the main work is to construct numerically the base functions of the unit cells. Take one of the coarse-grid elements shown in Fig. 2 for example, the element occupying a region \mathbf{K} , $\mathbf{K} \subset \Omega$. The base functions are constructed by solving the equilibrium equations in the region \mathbf{K} with some specified boundary conditions. From Eqs. 1 and 2, the general expression for solving of the base functions \mathbf{N}_i of a two-dimensional scalar field problem can be given as follows

$$\begin{aligned}
 \mathbf{L}\mathbf{N}_i &= 0 \text{ in } \mathbf{K} \\
 \mathbf{N}_i(\mathbf{x}) &\text{ affined on } \partial\mathbf{K} \\
 i &= 1, 2, \dots, d
 \end{aligned} \tag{4}$$

where, \mathbf{L} is the elasticity operator which satisfies $\mathbf{L}\mathbf{u} = \text{div} \left(\mathbf{D} : \frac{1}{2} \left(\nabla \mathbf{u} + (\nabla \mathbf{u})^T \right) \right)$, d is the number of nodes of the coarse-grid element.

For the vector field problems in solid mechanics, the multiscale base functions used for the displacement interpolation in different directions are no longer the same for the coarse-grid element with heterogeneous materials. The base functions must be constructed separately for each coordinate direction in order to consider the heterogeneities in a coarse-grid element, which is different from the multiscale base functions constructed for the scalar field problem.

Consider a two-dimensional vector field problem, as shown in Fig. 2. Two kinds of base functions for the interpolation of displacement field need to be constructed, in which one is used for the displacement interpolation in x -direction (N_x), and the other is used for the y -direction (N_y). Moreover, the deformations in different directions of a coarse-grid element depend upon each other due to the small-scale heterogeneous features within the coarse-grid element and the Poisson's effects. For this purpose, additional coupled terms (N_{yx}, N_{xy}) are introduced in the multi-scale base functions to consider the coupled effect among different directions in the multi-dimensional vector field problem [Zhang, Wu and Fu (2009); Zhang, Wu, Liu and Fu (2010)]. Consequently, the displacement interpolations of the coarse-grid element have the following forms

$$\begin{cases} u = \sum_{i=1}^d N_{ix} u'_i + \sum_{i=1}^d N_{iyx} v'_i \\ v = \sum_{i=1}^d N_{iy} v'_i + \sum_{i=1}^d N_{ixy} u'_i \end{cases} \quad (5)$$

i.e.

$$\mathbf{u} = \mathbf{N} \mathbf{u}'_{\mathbf{E}} \quad (6)$$

where, $N_{ix}|_j = \delta_{ij}$, $N_{iy}|_j = \delta_{ij}$, ($i, j = 1, 2, \dots, d$), δ is the Kronecker delta. N_{iyx} means the displacement field in the y -direction within the element induced by a unit displacement of node i in the x -direction. \mathbf{u} is the displacement vector of the nodes in the fine-scale mesh, \mathbf{N} is the base function matrix of the coarse-grid element, and $\mathbf{u}'_{\mathbf{E}}$ represents the displacement vector of nodes in macro level. They can be expressed as

$$\mathbf{u} = [u_1 \quad v_1 \quad u_2 \quad v_2 \quad \cdots \quad \cdots \quad u_n \quad v_n]^T$$

$$\mathbf{N} = [\mathbf{R}_1^T \quad \mathbf{R}_2^T \quad \cdots \quad \mathbf{R}_n^T]^T \quad (7)$$

$$\mathbf{u}'_E = [u'_1 \quad v'_1 \quad u'_2 \quad v'_2 \quad u'_3 \quad v'_3 \quad u'_4 \quad v'_4]^T$$

where

$$\mathbf{R}_i = \begin{bmatrix} N_{1x}(i) & N_{1xy}(i) & N_{2x}(i) & N_{2xy}(i) & N_{3x}(i) & N_{3xy}(i) & N_{4x}(i) & N_{4xy}(i) \\ N_{1yx}(i) & N_{1y}(i) & N_{2yx}(i) & N_{2y}(i) & N_{3yx}(i) & N_{3y}(i) & N_{4yx}(i) & N_{4y}(i) \end{bmatrix} \quad i = 1, 2, \dots, n \quad (8)$$

and n is the number of the nodes in the sub-grid mesh.

It can be verified that the base functions constructed above satisfy

$$\begin{cases} \sum_{i=1}^d N_{ix} = 1, & \sum_{i=1}^d N_{iy} = 1 \\ \sum_{i=1}^d N_{iyx} = 0, & \sum_{i=1}^d N_{ixy} = 0 \end{cases} \quad (9)$$

which ensures the rigid displacement of the coarse-grid element and the compatibility between the neighboring elements.

2.2.2 Equivalent stiffness matrix of coarse-grid element

Using the base functions constructed above, the equivalent stiffness matrix of a coarse-grid element can be given as [Zhang, Wu, Liu and Fu (2010);Zhang, Wu, Lv and Fu (2010)]

$$\mathbf{K}_E = \sum_{e=1}^m \mathbf{K}'_e, \quad \mathbf{K}'_e = \mathbf{G}_e^T \mathbf{K}_e \mathbf{G}_e \quad (10)$$

where \mathbf{K}_e is element stiffness matrix of an arbitrary fine-grid element e within the coarse-grid element shown in Fig. 2. m is the total number of the elements within the sub-grid mesh. \mathbf{G}_e , the transition matrix which denotes the mapping relations between the displacement vectors of micro-scale nodes and macro-scale nodes, can be expressed as

$$\mathbf{G}_e = [\mathbf{R}_{e1}^T \quad \mathbf{R}_{e2}^T \quad \dots \quad \mathbf{R}_{ed}^T]^T \quad (11)$$

2.3 Macro-scale computation

Once the equivalent element stiffness matrices of all the coarse-grid elements are derived, the standard FEM is then able to be carried out on the coarse-scale mesh.

The global stiffness matrix of the overall structure is obtained as follows [Zhang, Wu, Liu and Fu (2010); Zhang, Wu, Lv and Fu (2010)]

$$\mathbf{K} = \mathbf{A}_{i=1}^M \mathbf{K}_E^i \quad (12)$$

where $\mathbf{A}_{i=1}^M$ is a matrix assembled operator, and M is the total number of the coarse-grid elements. \mathbf{K}_E^i can be obtained from Eq.10.

Thus, a classical finite element analysis is implemented on the coarse-scale mesh, and the macroscopic displacement vector is given by

$$\mathbf{K}\mathbf{U} = \mathbf{F}_{ext} \quad (13)$$

where \mathbf{F}_{ext} is a vector of external forces subjected to the structure.

3 EMsFEM for Closed Liquid Cell Materials

3.1 Construction of the numerical base functions

Different from the general heterogeneous materials, the closed liquid cell materials are multiphase materials, which have closed inclusions fully filled with incompressible fluid. In order to fully capture and bring the small-scale information of both the solid structure and the fluid to the large scale, not only the numerical base functions for the displacement field are needed, but also the appropriate functions need to be constructed for the interpolation of the pressure field of the fluid phase. It should be remarked here that in the current study we assume that there will be no cavitation when a closed liquid cell is under tension state. Consequently, two sets of base functions are constructed respectively for each coarse-grid element. One set is used for the interpolation of the displacement field of the solid matrix, while the other is used for the interpolation of the fluid pressure caused by the deformation of the solid matrix. Thus, the complex coupling problems can be effectively solved on the coarse-scale mesh with great saving of computational efforts. Meanwhile, based on these two types of numerical base functions, the EMsFEM can execute easily the downscaling computation of the closed liquid cell materials.

Firstly, we describe the construction procedure of the multiscale base functions based on the four-node quadrilateral coarse-grid elements for the unit cell of the closed liquid cell materials. The more reasonable higher order element will be introduced in Section 3.4. As illustrated in Fig. 3, the green region within the unit cell represents a liquid inclusion. The numerical base functions with coupled additional terms for the interpolation of the displacement field of the closed liquid

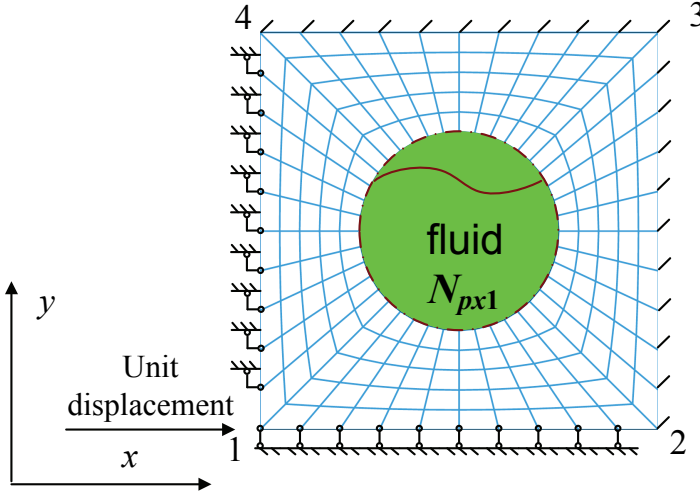


Figure 3: Linear boundary conditions for the construction of base functions $N_{1,x}$ of the four-node quadrilateral element

cell can be expressed as

$$\begin{cases} u = \sum_{i=1}^4 N_{ix}u'_i + \sum_{i=1}^4 N_{iyx}v'_i \\ v = \sum_{i=1}^4 N_{iy}v'_i + \sum_{i=1}^4 N_{ixy}u'_i \end{cases} \quad (14)$$

As the fluid inside the cell is incompressible, the volume of the cell satisfies the following condition

$$V_0 - V(u_k, v_k) = 0 \quad \text{on } \partial\Omega_{\text{in}} \quad (15)$$

where V and V_0 are the current and initial volumes of the fluid cell, respectively. Both V and V_0 can be calculated from the actual positions of the nodal points at the solid-liquid interface $\partial\Omega_{\text{in}}$.

The condition of incompressibility of Eq.15 can be incorporated in the potential energy expression by using the Lagrange multiplier method

$$\Pi^* = \Pi - \lambda(V - V_0) \quad (16)$$

where Π is the potential energy expression of the structure without the fluid inclusion, Π^* is the modified potential energy expression, λ is the Lagrange multiplier.

As pointed out by Ken-ichiro, Kozo and Masanori (1991), the hydrostatic pressure (P) of the fluid coincides with the Lagrange multiplier, i.e.

$$P = \lambda \quad (17)$$

Using the numerical base functions for the fluid pressure field, the pressure P inside the closed liquid cell can be expressed as

$$P = \sum_{i=1}^4 N_{pxi} u'_i + \sum_{i=1}^4 N_{pyi} v'_i \quad (18)$$

where N_{pxi} and N_{pyi} are the numerical pressure base functions, which mean the fluid pressures within the unit closed liquid cell induced by the unit displacements of node i in the x - and y -directions, respectively.

3.2 Linear boundary conditions

The linear boundary conditions, where $\mathbf{N}_i(\mathbf{x})$ varies linearly along $\partial\mathbf{K}$ (Eq.4) just as that in the standard bilinear base functions, are generally used in the MsFEM. Zhang et al. (2009) introduced simple linear boundary conditions for the construction of the base functions of solid skeleton of the heterogeneous saturated porous media. Furthermore, modified linear boundary conditions were proposed by Zhang, Wu and Fu (2010); Zhang, Wu, Lv and Fu (2010)] for the general vector field problems of heterogeneous media. In what follows, firstly, we will choose the modified linear boundary conditions to construct the numerical base functions for the analysis of the closed liquid cell materials. A type of more reasonable boundary conditions will be introduced in Section 4.

Fig. 3 gives illustration for the construction of N_{1x} , N_{1xy} and N_{px1} . For the linear boundary conditions, a unit displacement is applied on node 1 in the x -direction and the values vary linearly along boundaries 14 and 12, just as the bilinear shape functions in the standard FEM. At the same time, the nodes on boundaries 34 and 23 are fixed in the x -direction. The displacements of all boundary nodes in the sub-grid mesh are constrained in the y -direction. Using the boundary conditions mentioned above and by Eq.16, the internal displacement field of the unit cell and the pressure of fluid inside the cell can be solved directly on the sub-grid mesh by the standard FEM, thus the numerical base functions N_{1x} , N_{1xy} and N_{px1} can be obtained. The rest of the base functions of the unit cell can be constructed in a similar numerical procedure.

It can be verified that the above constructed numerical base functions satisfy

$$\begin{cases} \sum_{i=1}^4 N_{ix} = 1, \sum_{i=1}^4 N_{iy} = 1 \\ \sum_{i=1}^4 N_{ixy} = 0, \sum_{i=1}^4 N_{iyx} = 0 \\ \sum_{i=1}^4 N_{pxi} = 0, \sum_{i=1}^4 N_{pyi} = 0 \end{cases} \quad (19)$$

which guarantee the rigid body displacements of the coarse-grid element.

3.3 Treatment of volume expansion of the fluid in the unit cell

In the step of macro-scale computation as discussed in Section 2.3, the finite element analysis is performed on the coarse-scale mesh. Thus, all the external forces F_{ext} must be applied on the macroscopic nodes. However, in the real application of the closed liquid cell materials, some external forces act within the unit cells. Specially, the volume expansion, which can be considered as the driving forces for the closed liquid cells, acts on the fluid within the unit cells, as shown in Fig. 4. In what follows, the treatment of volume expansions of the fluid in the unit cells will be discussed.

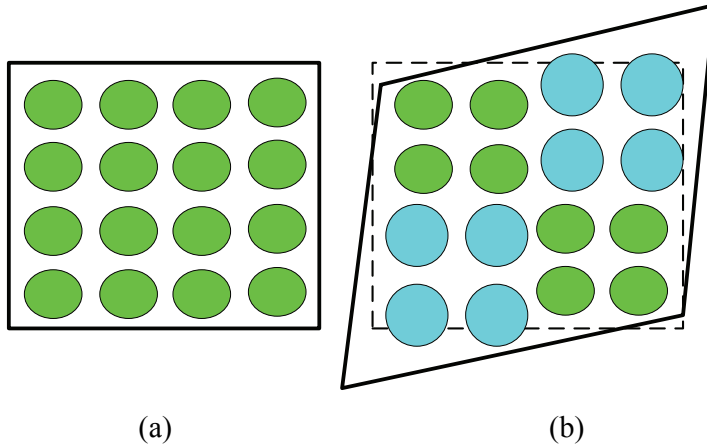


Figure 4: Closed liquid cells structures: (a) Initial state and (b) after local actuation

As shown in Fig. 5, a volume expansion ΔV_{fluid} is applied on the fluid within a unit cell. The main objective here is to determine how the volume expansion can be equivalently transformed to the macroscopic nodal forces. These macroscopic

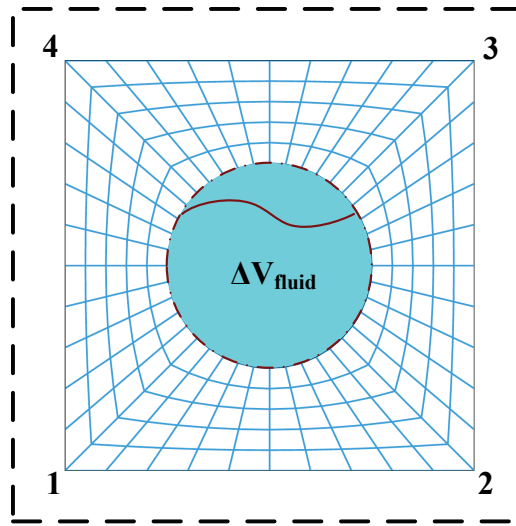


Figure 5: Closed liquid cell with volume expansion ΔV_{fluid}

equivalent forces are applied on the nodes in the coarse-scale mesh of the closed liquid cell materials.

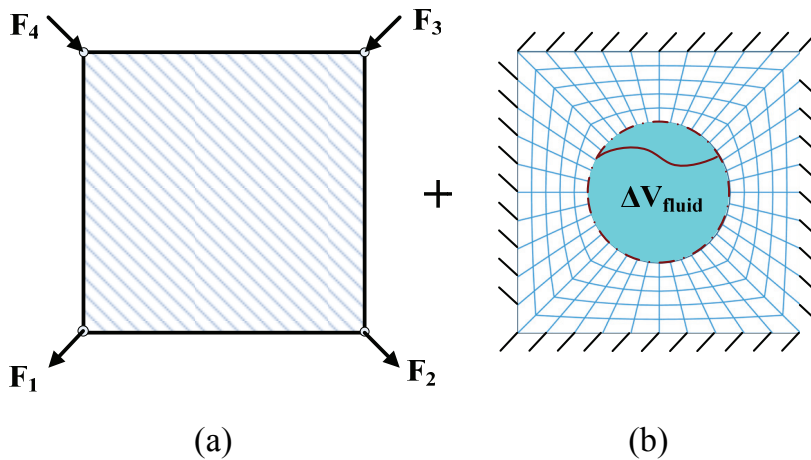


Figure 6: Equivalence of volume expansion of the fluid in the unit cell depicted in Fig. 5. (a) Macroscopic equivalent forces and (b) the boundary conditions for the calculation of the local response of the volume expansion

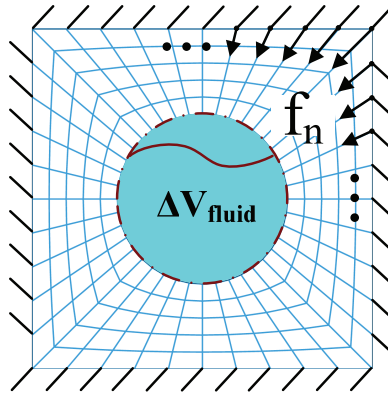


Figure 7: Approach to calculate macroscopic equivalent forces of the four-node quadrilateral element

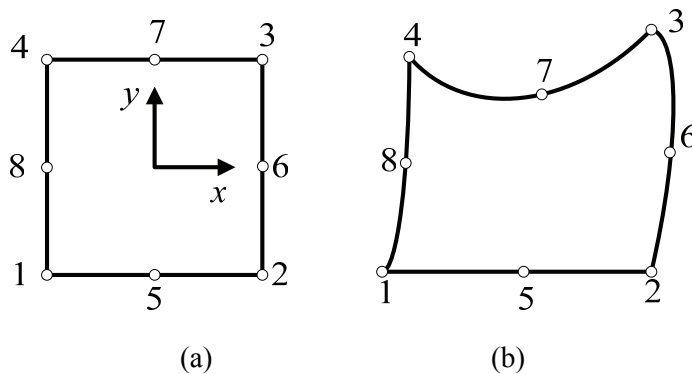


Figure 8: Eight-node quadrilateral coarse-grid element in the EMsFEM: (a) Initial state and (b) deformed state

The effects of the volume expansion of the fluid in the cells are treated as the combination of the effects of the macroscopic equivalent forces on the full structure and the local response of the volume expansion on the unit cell, as illustrated in Fig. 6. The macroscopic displacement field is solved under the macroscopic equivalent forces (see Fig. 6a), and the local response is calculated on the sub-grid of the unit cell under volume expansion with appropriate boundary conditions (see Fig. 6b). Due to the complexity of the closed liquid cell materials, there seems to be no analytical solution for the macroscopic equivalent forces. Consequently, a

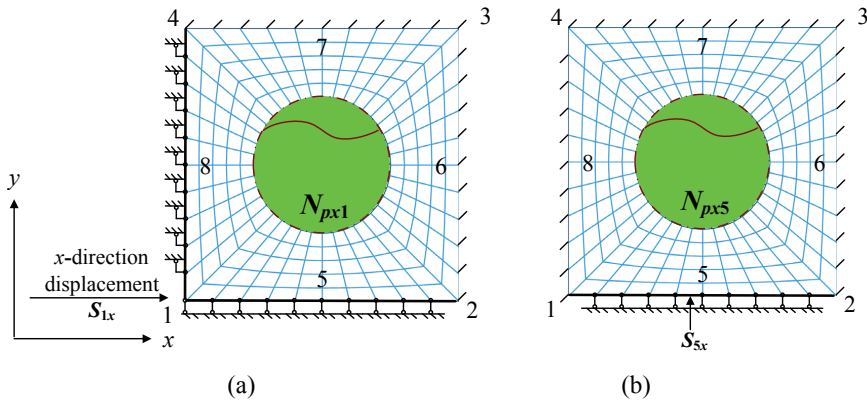


Figure 9: Boundary conditions for the construction of the base functions: (a) N_{1x} and (b) N_{5x} of the eight-node quadrilateral element

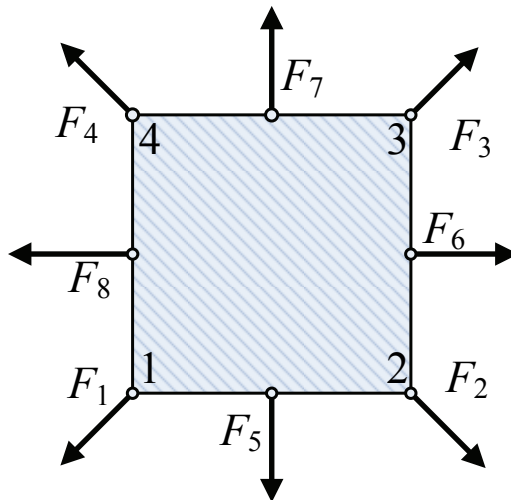


Figure 10: Approach to calculate macroscopic equivalent forces of the eight-node quadrilateral element

numerical method is used to derive the macroscopic equivalent forces. When the linear boundary conditions are adopted to construct the base functions, the overall procedure of the method can be divided into three steps:

Step1: The nodes at all the boundaries of the unit cell are constrained. Meantime,

a unit volume expansion ΔV_{fluid} is applied on the fluid in the unit cell. With these boundary and loading conditions, the nodal forces \mathbf{f}_n at the boundary nodes, as illustrated in Fig. 7, can be calculated by solving the equilibrium equation (i.e., Eq.1) on the sub-grid mesh with the standard FEM.

Step2: It is intuitive that the macroscopic equivalent forces will act on all four nodes of the corresponding coarse-grid element. The nodal forces \mathbf{f}_n at the boundary nodes are the distributed form of the macroscopic equivalent forces and can be converted to the corresponding equivalent forces ($\mathbf{F}_{Eix,n}, \mathbf{F}_{Eiy,n}$) at the corner nodes of the unit cell by [Zhang, Wu and Fu (2010)]

$$[\mathbf{F}_{Eix,n} \quad \mathbf{F}_{Eiy,n}] = [f_{nx} \quad f_{ny}] \begin{bmatrix} N_{ix}^n & N_{iyx}^n \\ N_{ixy}^n & N_{iy}^n \end{bmatrix} \quad (20)$$

where, $i = 1, 2, 3, 4$.

Step3: Based on the equivalent forces, the macroscopic equivalent forces can be calculated by

$$\mathbf{F} = - \sum_{n \in \partial \Omega_e} \mathbf{F}_{E,n} \quad (21)$$

Now, let's discuss the solution for the local effects of the volume expansion of the fluid in the unit cell. With the linear boundary conditions, the local effects can be calculated by constraining the boundary nodes in the sub-grid in both the x - and y -directions, as shown in Fig. 7. Thus, the local effects (i.e. displacement, stress, strain and pressure of the unit cell) of the volume expansion can be obtained by the standard FEM on the sub-grid mesh with the boundary conditions mentioned above.

3.4 Higher order element for the EMsFEM

As indicated by the numerical experiments (see the results given in Section 5), the EMsFEM with the four-node quadrilateral coarse-grid elements sometimes will induce strong boundary effects and cannot predict accurately the fluid pressure in the closed cells. The reason is that the linear boundary conditions for the construction of the numerical base functions in the EMsFEM impose too strong restriction on the boundary layer deformation of the coarse-grid element. To reduce the boundary effects, the oversampling techniques [Hou and Wu (1997); Hou, Wu and Cai (1999); Zhang, Wu and Fu (2009); Zhang, Wu, Liu and Fu (2010)] were generally proposed to introduce oscillatory boundary conditions for constructing the more reliable base functions in both the MsFEM and the EMsFEM. These oversampling techniques provide an effective approach to remove the resonance effect between the mesh

scale and the physical scale of the general heterogeneous problems. However, from our numerical experiences, it is found that there would be some difficulties when the oversampling techniques are extended to deal with the problems in the closed liquid cell materials.

To overcome these difficulties, in the current study, a more reasonable higher order element corresponding to the coarse-grid element is proposed for the EMsFEM to reduce the boundary effects. This type of element consists of eight nodes (see Fig. 8), which are all located on the boundaries of the unit cell. The procedure for the construction of the numerical base functions can be defined as follows.

Unlike the four-node quadrilateral coarse-grid element mentioned above, there are more than two nodes located on each edge of the eight-node quadrilateral coarse-grid element. Thus, the linear boundary conditions can not be applied on the unit cell to construct the numerical base functions. In contrast, quadratic boundary conditions are introduced, just as that used in the construction of the base functions of the eight-node quadrilateral element in the standard FEM.

Without loss of generality, take a unit closed liquid cell as an example (see Fig. 9), N_i denotes the base function of node i , S_i represent the corresponding boundary conditions for the construction of N_i . Our task is to define an appropriate S_i to resolve the base function N_i , which satisfies $N_{ix}|_j = \delta_{ij}, (i, j = 1 \sim 8)$. In accordance with the choice of quadratic base functions of the higher order element in the standard FEM, the boundary conditions S_i for the construction of the numerical base functions of the eight-node quadrilateral coarse-grid element need to follow the quadratic form. Taking the construction of N_{1x} for example, we note that $N_{1x} = 1$ at node 1 and $N_{1x} = 0$ at other nodes. In addition, N_{1x} has to vanish along the edges 43 and 23. Consequently, the corresponding quadratic boundary condition for all the edges in the x -direction can be expressed as

$$s_{1x} = -\frac{1}{4} \left(1 - \frac{x}{a}\right) \left(1 - \frac{y}{b}\right) \left(1 + \frac{x}{a} + \frac{y}{b}\right) \quad (22)$$

Meanwhile, the boundary nodes in the sub-grid mesh are all constrained in the y -direction, as shown in Fig. 9a. Using all the conditions mentioned above, the internal displacement field of the coarse-grid element and the pressure of the fluid within the unit cell can be calculated by the standard finite element analysis on the sub-grid mesh of the unit cell. Thus the numerical base functions N_{1x} , N_{1xy} and N_{px1} are obtained.

The other base functions (N_2 , N_3 and N_4) at the corner nodes of the coarse-grid element can be constructed in a similar way, while there is a little difference for constructing the base functions N_5 , N_6 , N_7 and N_8 at the midpoints. For instance, N_{5x} vanishes along the edges 43, 23 and 14, as shown in Fig. 9b. The quadratic

boundary condition for N_{5x} thus has to be of the form

$$s_{5x} = \frac{1}{2} \left(1 - \left(\frac{x}{a} \right)^2 \right) \left(1 - \frac{y}{b} \right) \quad (23)$$

It can be verified that the base functions constructed above satisfy

$$\begin{cases} \sum_{i=1}^8 N_{ix} = 1, \sum_{i=1}^8 N_{iy} = 1 \\ \sum_{i=1}^8 N_{ixy} = 0, \sum_{i=1}^8 N_{iyx} = 0 \\ \sum_{i=1}^8 N_{pxi} = 0, \sum_{i=1}^8 N_{pyi} = 0 \end{cases} \quad (24)$$

which ensure the rigid displacement of the coarse-grid element and the compatibility between the neighboring elements.

Once the base functions are constructed, the displacement field and the pressure of the fluid within the unit closed liquid cell can be expressed as

$$\begin{cases} u = \sum_{i=1}^8 N_{ix} u'_i + \sum_{i=1}^8 N_{iyx} v'_i \\ v = \sum_{i=1}^8 N_{iy} v'_i + \sum_{i=1}^8 N_{ixy} u'_i \\ P = \sum_{i=1}^8 N_{pxi} u'_i + \sum_{i=1}^8 N_{pyi} v'_i \end{cases} \quad (25)$$

For the eight-node quadrilateral coarse-grid element, the macroscopic equivalent forces which are used to substitute the volume expansion of the fluid will be not only applied on the corner nodes, but also act on the middle nodes of the higher order coarse-grid element, as illustrated in Fig. 10. The solution of the macroscopic equivalent forces and the local effects of the volume expansions can be performed in a similar way as those for the four-node quadrilateral coarse-grid element mentioned before.

4 Periodic boundary conditions

Numerical experiments have shown that the EMSFEM with the higher order element and oversampling technique could generate better results than the conventional EMSFEM. However, it was also found that the EMSFEM with higher order element technique and oversampling technique sometimes will still have low accuracy when the coarse mesh scale is close to the physical scale.

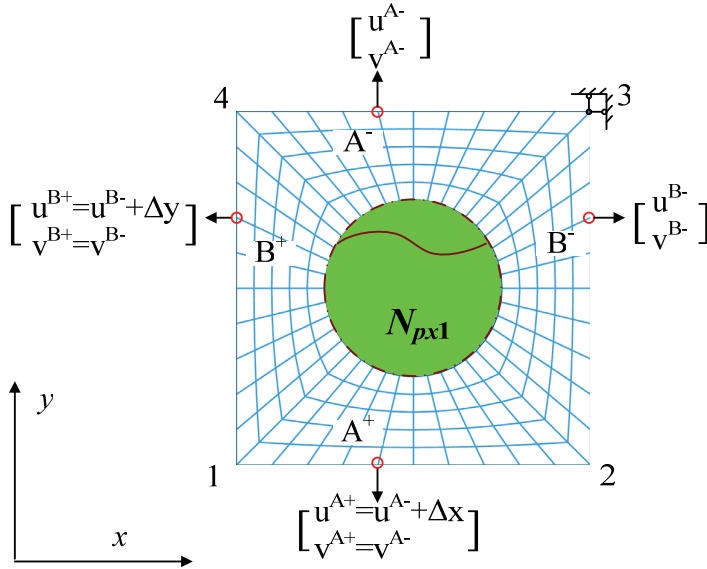


Figure 11: Periodic boundary conditions for the construction of the base function N_{1x} of the four-node quadrilateral element

To alleviate these difficulties, a novel approach based on the periodic boundary conditions is introduced to construct the numerical base functions. Firstly, the treatment is explained with the conventional four-node quadrilateral element [Zhang, Wu, Lv and Fu (2010)]. Then, the periodic boundary conditions are developed for the construction of the numerical base functions of the higher order element in the EMsFEM.

4.1 Periodic boundary conditions for the four-node quadrilateral element

Let us consider a structure consisting of a periodic array of RVEs. Since the periodic array represents a continuous physical body, two continuities (displacement and traction distributions) must be satisfied at the boundaries between the neighboring RVEs. Based on these continuities, the unified periodic boundary conditions have been developed in the conventional homogenization method to predict the mechanical response of composites materials. Motivated by this concept, Zhang and his coworkers [Zhang, Wu, Lv and Fu (2010)] assume that the local periodicity of the morphology is still applicable in the EMsFEM for the analysis of the periodic structures. Thus, a novel approach based on the periodic boundary conditions was

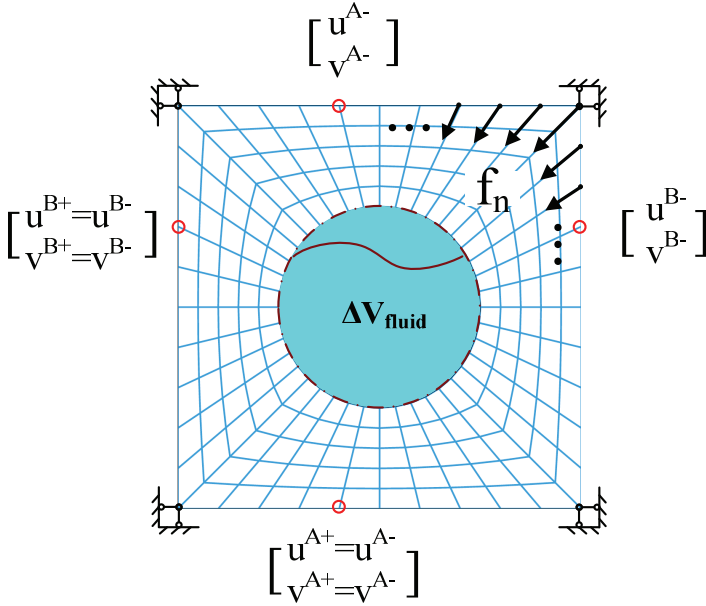


Figure 12: Periodic boundary conditions for the calculation of the macroscopic equivalent forces of the four-node quadrilateral element

developed for the construction of the numerical base functions. In the current work, the same approach is implemented to construct the numerical base functions of the closed liquid cell. The main procedure can be described as below.

Consider a closed liquid unit cell with vertices 1, 2, 3 and 4 that are interconnected by boundaries Γ_{12} , Γ_{23} , Γ_{43} and Γ_{14} , as shown in Fig. 11. Instead of the prescribed displacements which are common in the linear boundary conditions, kinematical constraints are applied to the boundaries to ensure periodicity of the model in the deformed configuration. Take the construction of N_{1x} for example, as illustrated in Fig. 11, the boundary conditions for a pair of the corresponding nodes (A^+, A^-) on opposite edges Γ_{12} and Γ_{43} , can be given as

$$\begin{cases} u^{A^+} - u^{A^-} = \Delta x \\ v^{A^+} = v^{A^-} \end{cases} \quad (26)$$

Similarly, for a pair of the corresponding nodes (B^+, B^-) on the opposite edges Γ_{14}

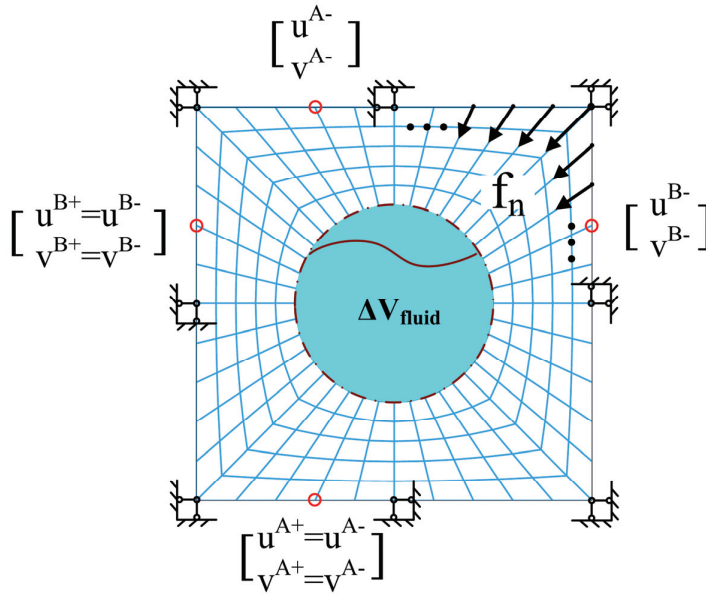


Figure 13: Periodic boundary conditions for the construction of the base function N_{1x} of the eight-node quadrilateral element

and Γ_{23} , the boundary conditions can be expressed as

$$\begin{cases} u^{B+} - u^{B-} = \Delta y \\ v^{B+} = v^{B-} \end{cases} \quad (27)$$

where, Δx and Δy are given constants, whose values at node 1 are both set to be 1, and are both set to be zero at nodes 2 and 4. For the other nodes, the values of Δx and Δy vary linearly along edges Γ_{12} and Γ_{14} , respectively. The displacements of the node 3 are constrained in both directions. Using the kinematical constraints described above, the whole displacement field of the coarse-grid element can be obtained by solving the equilibrium equation (Eq.1) on the sub-grid mesh with the standard FEM. The numerical base function N_{1x} is then obtained.

Under the periodic boundary conditions, the treatment of the volume expansions is almost the same as that under the linear boundary conditions. However, it is obvious that those fix constraints (i.e., the nodes at the boundaries are all constrained, as shown in Fig. 7) used in the linear boundary conditions are not suitable for resolving the macroscopic equivalent forces and the local effects of the volume expansion of the fluid upon the periodic boundary conditions. Consequently, instead

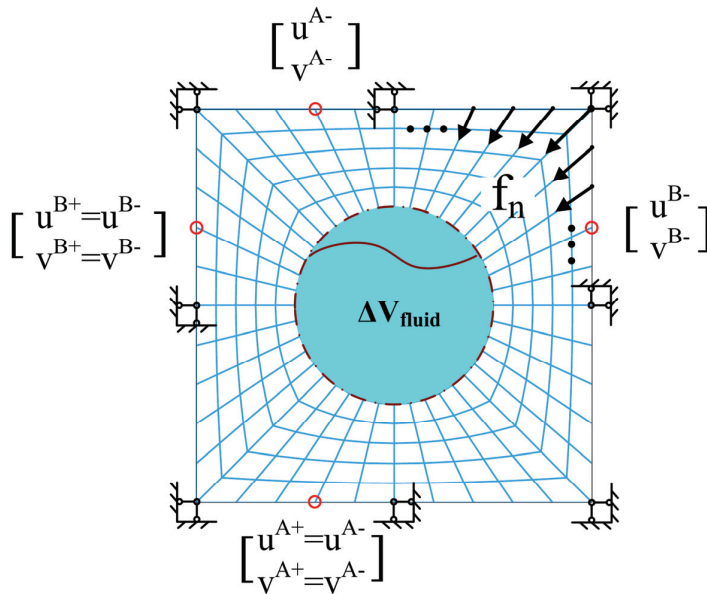


Figure 14: Periodic boundary conditions for the calculation of the macroscopic equivalent forces of the eight-node quadrilateral element

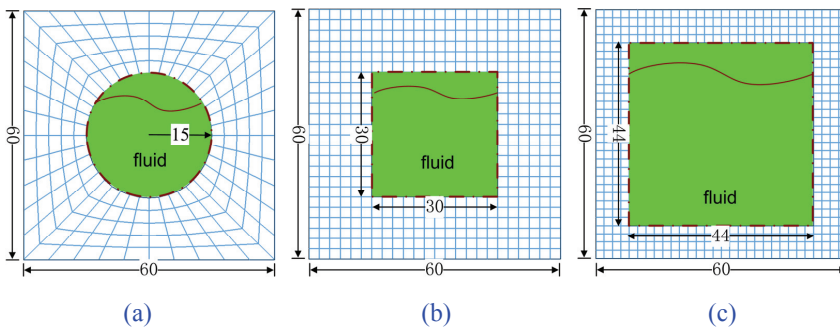


Figure 15: Microscopic models of (a) Unit cell A, (b) Unit cell B and (c) Unit cell C

of the fixed constraints, the corresponding periodic boundary conditions are applied on the unit cell to calculate the macroscopic equivalent forces and the local effects. The detail of this procedure is illustrated in Fig. 12. Only the four corner nodes are fixed, while the other nodes on the edges are constrained periodically. For exam-

ple, the boundary conditions for a pair of the corresponding nodes (A^+, A^-) on the opposite edges can be given as:

$$\begin{cases} u^{A^+} = u^{A^-} \\ v^{A^+} = v^{A^-} \end{cases} \quad (28)$$

Using the boundary conditions described above, the nodal forces \mathbf{f}_n at the boundary nodes can be calculated by solving the equilibrium equation (i.e., Eq.1) on the sub-grid mesh with the standard finite element analysis. Then, the macroscopic equivalent forces can be calculated by Eqs. 20 and 21 as mentioned above.

4.2 Periodic boundary conditions for the higher order element

In this subsection, the generalized periodic boundary conditions are introduced to construct the base functions of the higher order element. Similar to the periodic boundary conditions used in the conventional four-node quadrilateral element, the kinematical constraints are applied to nodes on the opposite boundaries of the eight-node quadrilateral element to ensure periodicity of the model in the deformed configuration. In particular, the nodes at the center of the edges of the unit cell, i.e. the middle nodes of the higher order element, need to be fixed to ensure that the base functions obtained can satisfy $N_{ix}|_j = \delta_{ij}$, ($i, j = 1 \sim 8$). Take the construction of the N_{1x} for example, the boundary conditions are shown in Fig. 13. The boundary conditions for a pair of corresponding nodes (A^+, A^-) can be also expressed as Eq.26. But now, the values of Δx are given as

$$\Delta x = -\frac{1}{4} \left(1 - \frac{x}{a}\right) \left(1 - \frac{y}{b}\right) \left(1 + \frac{x}{a} + \frac{y}{b}\right) \quad (29)$$

Moreover, nodes 3, 6 and 7 need to be constrained in all directions. Using these boundary conditions, the base function N_{1x} can be calculated on the sub-grid mesh by the standard FEM. The rest of the base functions can be constructed in a similar way. It can be verified that the base functions obtained satisfy Eq.24.

The treatment of the volume expansion of the fluid in the unit cells for the higher order element under the periodic boundary conditions can be performed in a similar way as that described for the conventional four-node quadrilateral element. The corresponding boundary conditions can be found in Fig. 14.

5 Numerical experiments

In this section, several representative numerical examples are presented to assess the accuracy of the proposed EMsFEM for the analysis of the closed liquid cell

materials. Four strategies, i.e. the EMsFEM based on the four-node quadrilateral coarse-grid elements with the linear boundary conditions (EMsFEM-4), the EMsFEM based on the four-node quadrilateral coarse-grid elements with the periodic boundary conditions (EMsFEM-4P), the EMsFEM based on the eight-node quadrilateral coarse-grid elements with the quadratic boundary conditions (EMsFEM-8) and the EMsFEM based on the eight-node quadrilateral coarse-grid elements with the periodic boundary conditions (EMsFEM-8P) are implemented. The results obtained are compared with those calculated by the standard FEM with conventional four-node elements (FEM-4) or conventional eight-node elements (FEM-8) applied on the fine-scale mesh. The closed cell structure considered is composed of $n_x \times n_y = 20 \times 6$ periodic unit cells where n_x and n_y denote the numbers of unit cells in the x - and y -directions, respectively. Moreover, in order to examine the accuracy of the EMsFEM developed for the closed liquid cell structure more intuitively, three types of unit cells are considered. The size and the fine-scale mesh of these unit cells are shown in Fig. 15. Plane strain condition is assumed in the study, and all the parameters used in the examples are dimensionless. The Young's modulus is $2.0E9$ and the Poisson's ratio is 0.3 .

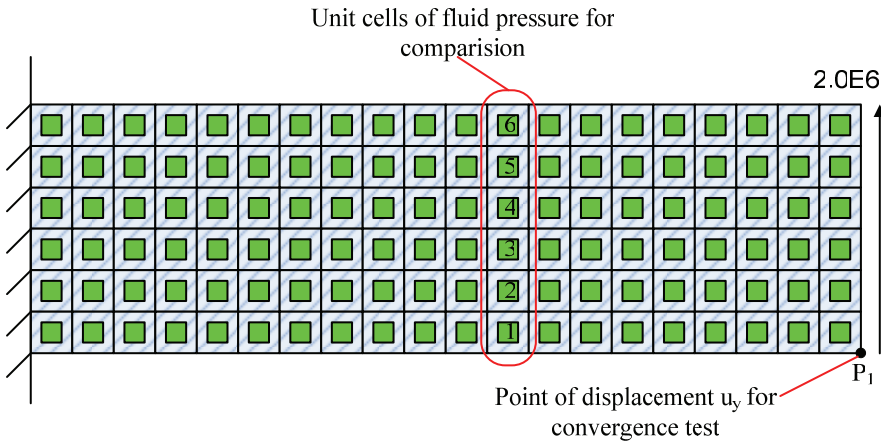
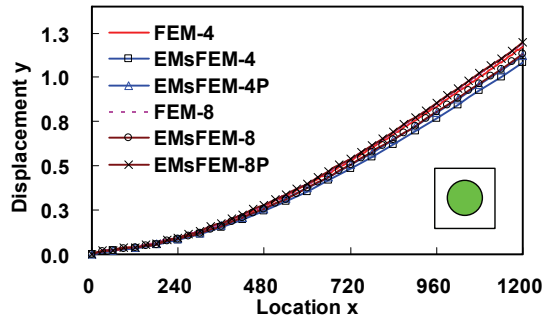
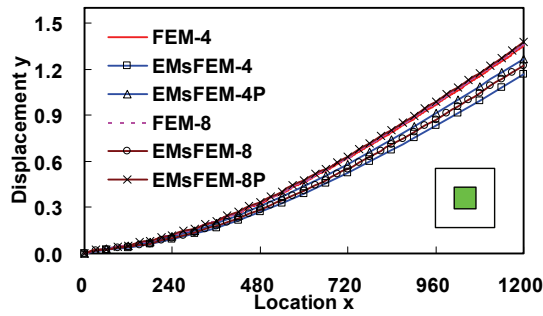


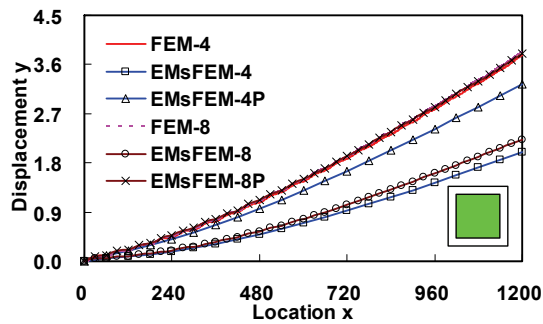
Figure 16: The boundary conditions for the structure with 20×6 closed liquid cells subjected to external loads



(a)



(b)



(c)

Figure 17: Displacements in the y-direction of the points on the bottom surface of the cantilever closed liquid cell beam structure separately composed of (a) Cell A, (b) Cell B and (c) Cell C subjected to external forces

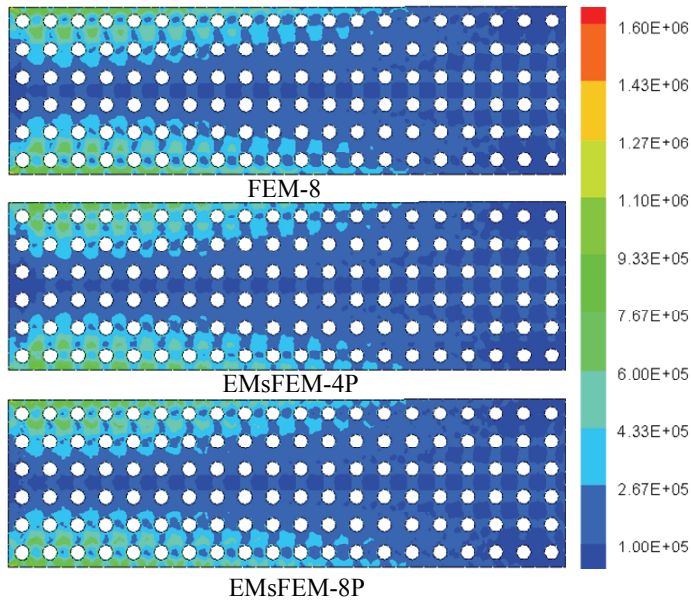


Figure 18: Microscopic von Mises stress of the whole structure

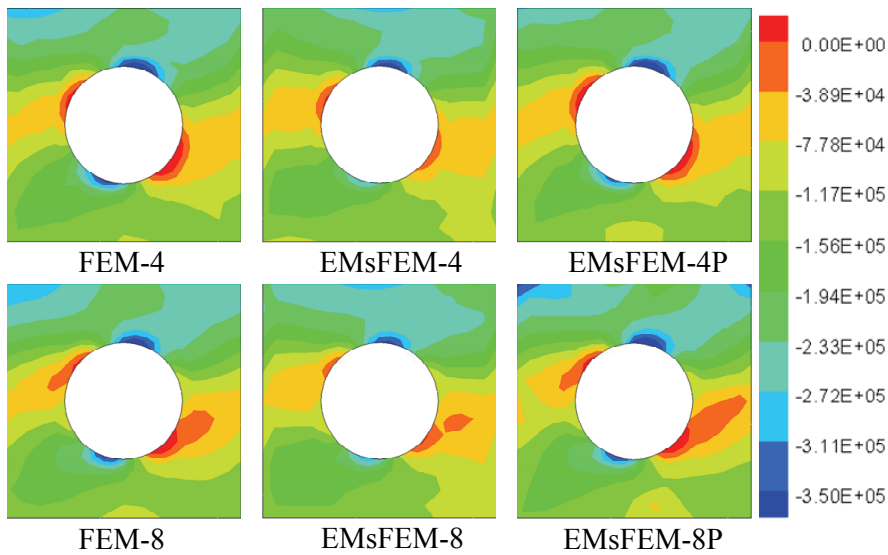


Figure 19: Microscopic stress in the x -direction of the unit cell 5 marked in Fig. 16

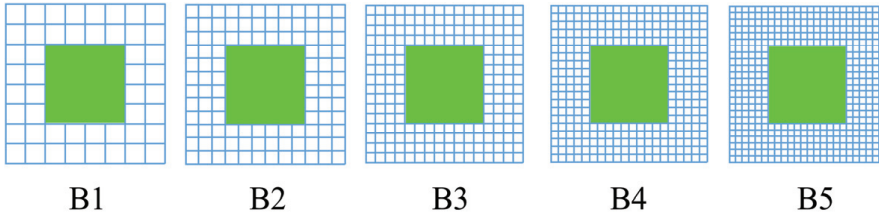


Figure 20: Five types of sub-grid mesh of Cell B

5.1 Mechanical simulation of the closed liquid cell structure subjected to external forces

As an assessment of the EMsFEM described previously for the analysis of the closed liquid cell structure, a comparison between the results calculated by the EMsFEMs and those obtained by the standard FEM is performed. Firstly, we assumed that the structure is only subjected to the external loads and there is no volume expansion of the fluid in all the cells of the structure. As illustrated in Fig. 16, the structure can be considered as a cantilever beam, of which the left side is fixed. The uniform distributed forces of $2.0E6$ act along the right side of the structure.

The displacements in the y -direction of the nodes on the bottom surface of the structure composed of three types of unit cells are illustrated in Figs. 17(a)-(c), respectively. It can be observed that the results obtained by the EMsFEM based on both four-node and eight-node quadrilateral elements in general agree well with the reference values obtained by the standard FEM (FEM-4 and FEM-8). Moreover, we can observe that the periodic boundary conditions play an important role in improving the accuracy of the EMsFEM. Comparing the results shown in Figs. 17(b) and (c), it can be seen that the accuracy of the EMsFEM-4 and the EMsFEM-8 becomes worse when the dimension of the inclusion is close to that of the unit cell. This is also called the “resonance effect” which is mainly induced by the boundary layer in the first-order corrector [Hou and Wu (1997); Hou, Wu and Cai (1999)]. In general, these errors can be alleviated by the periodic boundary conditions for general heterogeneous periodic materials [Zhang, Wu, Lv and Fu (2010)]. However, due to the special characteristic of the closed liquid cell structure, i.e. a fluid-filled inclusion inside the cell, the EMsFEM-4P still has large errors. On the other hand, it can be found that a good agreement of the results between the EMsFEM-8P and the standard FEM is obtained. This means that the EMsFEM-8P can obtain more satisfactory results.

Since the EMsFEM can take the downscaling computation easily, we can do the downscaling computations with the developed EMsFEM methods directly and com-

pare them with the standard FEM. For simplicity, we only take the downscaling computation of the structure consisting of a periodic array of Cell A (see Fig. 15a). The distribution of the microscopic von Mises stress in the whole structure is shown in Fig. 18. It can be observed that the EMsFEM-8P can reach acceptable results of the actual microscopic stress. In addition, the stress in the x -direction (σ_{11}) of the local unit cell (i.e., the No. 5 cell in Fig. 16) of the structure is plotted in Fig. 19. It can be found that the results obtained by the EMsFEM-8P fit fairly well those calculated by FEM-8.

Now let's discuss the errors of the pressure of the fluid within the closed cells in the structure. The error formula for the pressure of the fluid within the closed cells in the structure is defined as

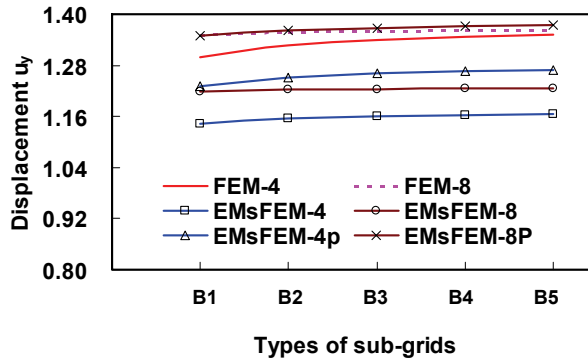
$$Err_i\% = \frac{|P_{FEM}^i - P_{EMsFEM}^i|}{|P_{FEM}^{Max}|} \times 100\% \quad (30)$$

where P_{FEM}^i is the pressure of the i -th unit cell in the structure obtained by the FEM, P_{EMsFEM}^i is the pressure calculated by the EMsFEM and $|P_{FEM}^{Max}|$ is the absolute value of maximal fluid pressure in all unit cells in the structure.

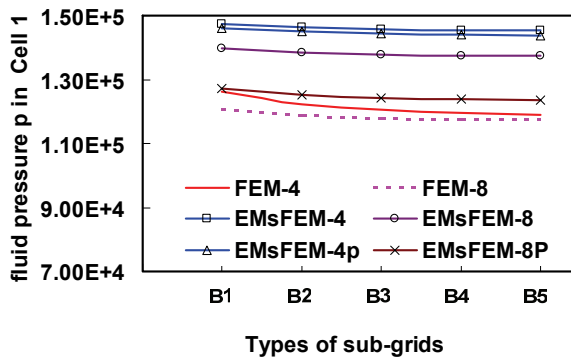
The errors of the fluid pressure calculated based on Eq.30 are listed in Tab. 1 for some unit cells. In general, we may find that the fluid pressures calculated by the EMsFEMs coincide well with the reference solutions. Furthermore, we can observe that the errors obtained by all the EMsFEM methods become larger when the location of the unit cells is closer to the boundary of the structure. This is called the "boundary effects", which are common to the conventional multi-scale/homogenization methods based on the local periodicity hypothesis. On the other hand, we can find that the errors of the fluid pressure calculated by the EMsFEM-8P are less than 1.41%. The boundary effects can be reduced effectively by using the higher order elements with periodic boundary conditions.

Table 1: Error analysis of the fluid pressure in some unit cells of the structure composed of unit cell B subjected to external forces

	EMsFEM-4	EMsFEM-4P	EMsFEM-8	EMsFEM-8P
Cell 1	8.11%	7.68%	5.68%	1.39%
Cell 2	0.92%	1.18%	0.40%	1.15%
Cell 3	0.42%	0.51%	0.17%	0.24%
Cell 4	0.40%	0.49%	0.16%	0.23%
Cell 5	0.91%	1.17%	0.38%	1.14%
Cell 6	8.13%	7.70%	5.69%	1.41%



(a)



(b)

Figure 21: Convergence rate of (a) the displacement u_y and (b) the fluid pressure p in Cell 1 as shown in Fig. 16 with refining the sub-grids of Cell B

5.2 Convergence test

In this test, we still consider the model used in Section 5.1, but only the Cell B (see Fig. 15b) is chosen. A series of mesh discretization schemes are conducted by stepwise refining the sub-grid mesh of the unit cells, as shown in Fig. 20. All the multiscale strategies developed in this paper (EMsFEM-4, EMsFEM-4P, EMsFEM-8 and EMsFEM-8P) are applied to simulate the structure, while both the standard FEMs (FEM-4 and FEM-8) are adopted to solve this problem on the fine-scale mesh. It should be mentioned here that the fine-scale mesh is also refined while refining the sub-grid mesh of the cell.

The results of the displacement in the y -direction (u_y) of Point P1 (see Fig. 16) are

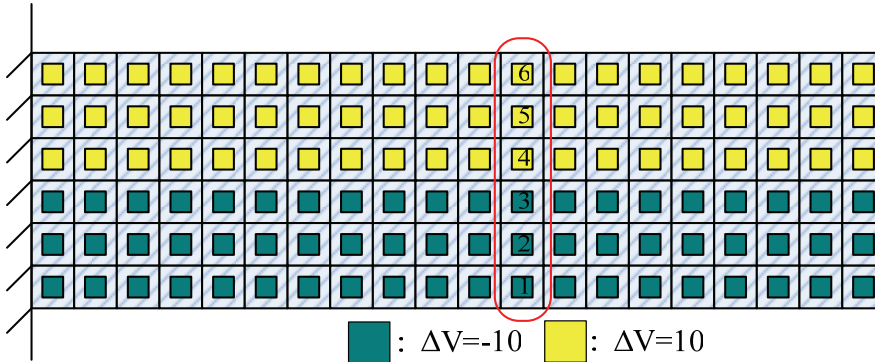


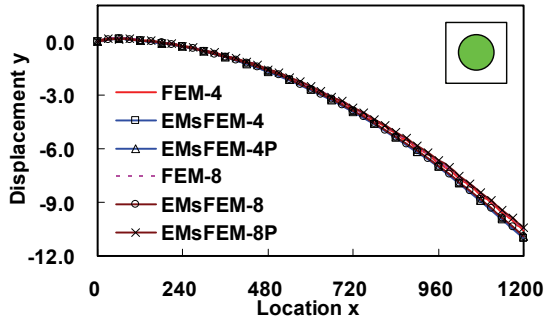
Figure 22: The boundary conditions for the structure with 20×6 closed liquid cells subjected to volume expansions

shown in Fig. 21(a). The results of the fluid pressure in one of the unit cell (Cell 1) are shown in Fig. 21(b). It can be observed that the results obtained by all the multiscale strategies converge monotonously. The same phenomenon can be found in the results calculated by the two standard FEMs when the mesh of the structure is stepwise refined. We also observe that the results calculated by the EMsFEM-8P agree better with the reference values obtained by FEM-8 than the other EMsFEMs.

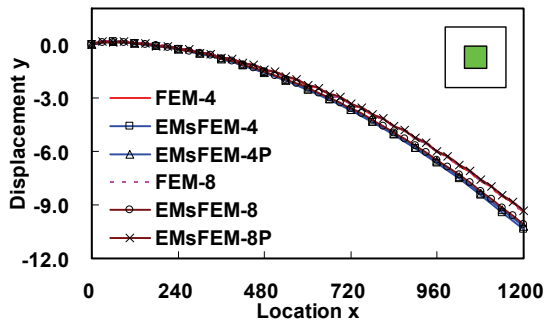
5.3 Mechanical simulation of the closed liquid cell structure subjected to volume expansions of the fluid

The closed liquid cell structures are materials that are capable of performing mechanical work in the form of physical shape change. The shape change can be directly controlled by changing the pressure and volume expansion of the fluid in the closed cells. Consequently, the accuracy of the treatment of the volume expansion of the fluid in unit cells is one of key factors for the survival and success of the EMsFEM for the mechanical analysis of the closed liquid cell materials. In this example, we are going to demonstrate the accuracy of the results of the deformation and the fluid pressure, which are calculated by the EMsFEM when the closed liquid cell structure is subjected to volume expansions. We continue to consider the cantilever liquid close cell beam structure with three types of unit cells mentioned in Section 5.1. An increase or decrease in the volumes of the fluid inclusions is applied to the structure, as depicted in Fig. 22.

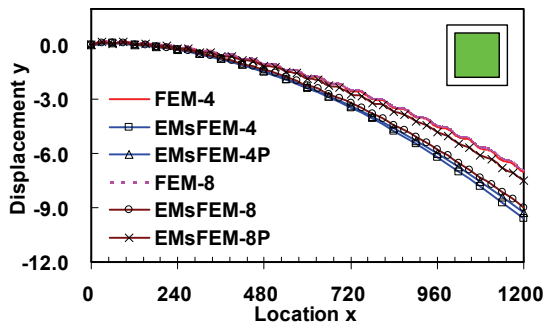
Figs. 23(a) and (c) plot the displacements in the y -direction of the nodes on the



(a)



(b)



(c)

Figure 23: Displacements in the y-direction of the points on the bottom surface of the cantilever closed liquid cell beam structure separately composed of (a) Cell A, (b) Cell B and (c) Cell C subjected to volume expansions

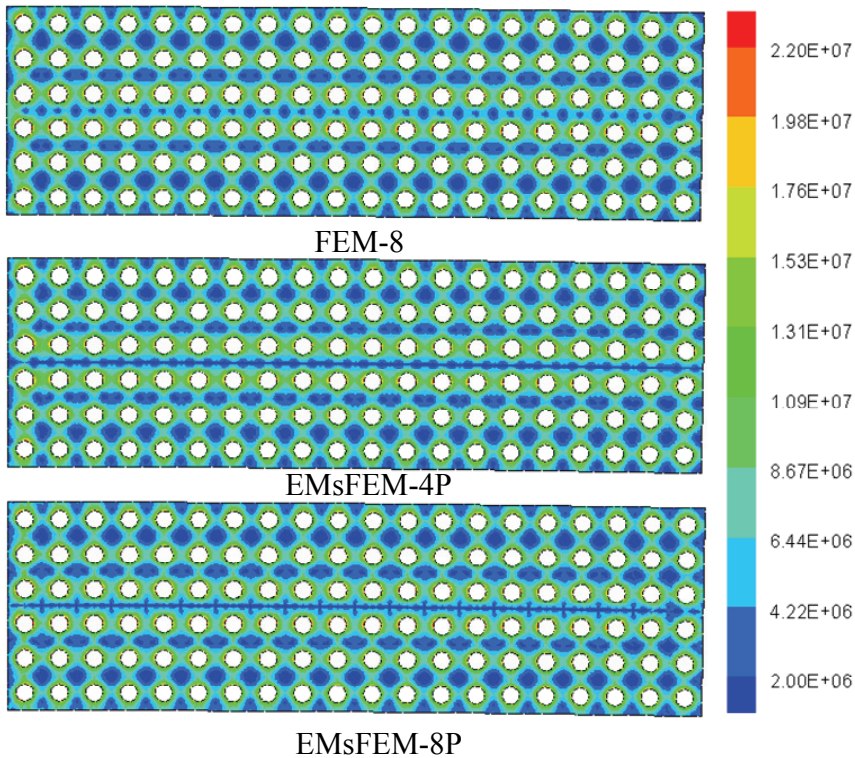


Figure 24: Microscopic von Mises stress of the whole structure

bottom surface of the structure with three types of unit cells, respectively. It can be observed that the results obtained by the EMsFEMs and those calculated by the two standard FEMs exhibit a good agreement with each other. This also means that the treatment of the volume expansion of the fluid works with acceptable accuracy. In particular, we can find from Fig. 23(c) that the errors of the EMsFEM-4 and the EMsFEM-4P are magnified when the dimension of the fluid inclusion is close to the size of the unit cell. Besides the resonance effect mentioned above, another important reason is that the boundary conditions for the calculation of the numerical base functions in the EMsFEM-4 and EMsFEM-4P impose relatively strong restrictions for the boundary nodes. The macroscopic equivalent forces can not be represent sufficiently well the real volume expansion. In contrast, since the nodes at the middle of the edges in the higher order elements are taken into account, the errors induced by the EMsFEM-8 are reduced. Furthermore, combining the periodic boundary conditions with the higher order elements, the EMsFEM-8P can

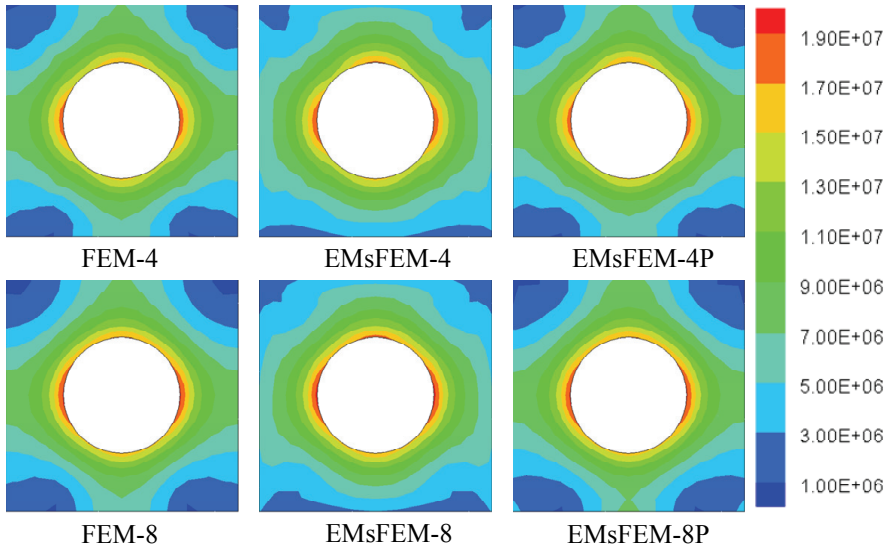


Figure 25: Microscopic von Mises stress of Cell 5 marked in Fig. 22

obtain more satisfactory results. It implies that the periodic boundary conditions proposed for the higher order elements can reflect better the heterogeneous behaviors of the coarse-grid elements and can simulate the boundary deformation of the closed liquid cell more reasonably under the volume expansion conditions of the fluid.

The downscaling computation of all the EMsFEM methods is conducted here and the results are compared with those calculated by the standard FEM. For simplicity, we still only consider the structure consisting of Cell A. The distribution of microscopic equivalent stress in the whole structure obtained by the FEM-8, EMsFEM-4P and EMsFEM-8P is shown in Fig. 24. In addition, the stress distribution of one of the unit cells in the structure (Cell 5 as shown in Fig. 22) is carried out in detail, as illustrated in Fig. 25. It can be observed that the EMsFEM-8P can acquire acceptable results of the actual microscopic stress in the closed liquid cell structure.

Furthermore, relatively larger errors of the fluid pressure obtained by the EMsFEM-4, EMsFEM-4P, and EMsFEM-8 can be observed in Tab. 2. The boundary effects are even magnified when the volume expansions are imposed to the structure. Moreover, it can be also observed that the errors of the fluid pressure in general appear a little higher than those of the displacement results, especially when the fluid inclusions are located at the boundary of the structure. One of the reasons is

Table 2: Error analysis of the fluid pressure in some unit cells of the structure composed of unit cell B subjected to volume expansions

	EMsFEM-4	EMsFEM-4P	EMsFEM-8	EMsFEM-8P
Cell 1	10.65%	5.83%	8.93%	1.42%
Cell 2	4.42%	0.91%	3.02%	3.24%
Cell 3	11.92%	6.12%	6.90%	5.56%
Cell 4	11.92%	6.11%	6.90%	5.56%
Cell 5	4.41%	0.92%	3.02%	3.25%
Cell 6	10.64%	5.83%	8.92%	1.41%

the “boundary effects”, which are common and hard to be eliminated in the conventional multiscale/homogenization methods based on local periodicity hypotheses. Another reason is that the errors of fluid pressure are generally one order higher than the displacement, just as that observed in the conventional finite element method, where the stress error is generally higher than that of the displacement. On the other hand, when the periodic boundary conditions are introduced in the construction of the base functions for the EMsFEM with higher order elements (EMsFEM-8P), the errors of the fluid pressure are reduced. Thus, the EMsFEM-8P can provide more reliable results, not only for the displacement but also the fluid pressure.

From the numerical examples above, we can see that the results obtained by all the EMsFEMs developed for the closed liquid cell materials compare well with the reference values calculated by the standard FEM on the fine-scale mesh. The results obtained by the EMsFEM-8P are better than those calculated by the EMsFEM-4, EMsFEM-4P and EMsFEM-8.

6 Conclusions

The extended multiscale finite element method is developed for the mechanical analysis of closed liquid cell materials. The base functions constructed numerically for the displacement field as well as the pressure of the incompressible fluid within the closed liquid cell are employed to establish the relationship between the macroscopic and microscopic variables, such as displacement, stress, strain and pressure. In the macroscopic process, the effects of the volume expansion of the fluid in the unit cells are treated as the combination of the effects of the macroscopic equivalent forces and the local response of the volume expansion on the unit cells.

Numerical examples show that the extended multiscale finite element method with

the conventional four-node quadrilateral coarse-grid elements sometimes will induce strong boundary effects and cannot predict accurately the fluid pressure in the closed cells. Thus a more reasonable higher order coarse-grid element (eight-node) which can characterize the structural deformations of the closed cells with greater accuracy is proposed. The quadratic boundary conditions are introduced for the construction of the numerical base functions of the eight-node quadrilateral coarse-grid element.

Furthermore, inspired by the periodic boundary conditions used in the conventional homogenization method, the generalized periodic boundary conditions are introduced for the construction of numerical base functions of higher order elements. The results indicate that the extended multiscale finite element method with the higher order elements as well as periodic boundary conditions has more accuracy and can be successfully used for solving the closed liquid cell problems.

Acknowledgement: The supports of the National Natural Science Foundation (11072051, 10721062, 90715037, 91015003, 10728205, 10902021), NSFC-JST (51021140004), the National Key Basic Research Special Foundation of China (2010CB832704) and the 111 Project (No.B08014) are gratefully acknowledged.

References

Aarnes, J. E. (2006): On the use of a mixed multiscale finite element method for greater flexibility and increased speed or improved accuracy in reservoir simulation. *Multiscale Modeling and Simulation*, vol. 2, no. 3, pp. 421–439.

Aarnes, J. E.; Krogstad, S.; Lie, K. A. (2006): A hierarchical multiscale method for two-phase flow based upon mixed finite elements and nonuniform coarse grids. *Multiscale Modeling and Simulation*, vol. 5, no. 2, pp. 337–363.

Babuska, I. (1976): Homogenization approach in engineering, *Computing Methods in Applied Sciences and Engineering* (Lecture Notes in Economics and Mathematical Systems), no. 134, Springer, Berlin, 1976, pp. 137–153.

Babuska, I.; Caloz, G.; Osborn, E. (1994): Special finite element methods for a class of second order elliptic problems with rough coefficients. *SIAM Journal of Numerical Analysis*, vol. 31, no. 4, pp. 945–981.

Babuska, I.; Osborn, E. (1983): Generalized finite element methods: Their performance and their relation to mixed methods. *SIAM Journal of Numerical Analysis*, vol. 20, no. 3, pp. 510–536.

Benssousan, A.; Lions, J. L.; Papanicoulau, G. (1978): *Asymptotic analysis for periodic structures*. North-Holland, Amsterdam.

- Berger, H.; Kari, S.; Gabbert, U.; Rodriguez-Ramos, R.; Guinovart, R.; Otero, J. A.; Bravo-Castillero, J.** (2005): An analytical and numerical approach for calculating effective material coefficients of piezoelectric fiber composites. *International Journal of Solids and Structures*, vol. 42, pp. 5692–5714.
- Dang, T. D.; Sankar, B. V.** (2008): Meshless local Petrov-Galerkin micromechanical analysis of periodic composites including shear loadings. *CMES: Computer modeling in engineering & sciences*, Vol. 26, no. 3, pp. 169–187.
- Efendiev, Y.; Ginting, V.; Hou, T. Y.; Ewing, R.** (2006): Accurate multiscale finite element methods for two-phase flow simulations. *Journal of Computational Physics*, vol. 220, pp. 155–174.
- Efendiev, Y.; Hou, T. Y.; Ginting, V.** (2004): Multiscale finite element methods for nonlinear problems and their applications. *Communications in Mathematical Sciences*, vol. 2, pp. 553–589.
- Fish, J.; Shek, K.; Pandheeradi, M.; Shephard, M.S** (1997): Computational plasticity for composite structures based on mathematical homogenization: theory and practice. *Computer Methods in Applied Mechanics and Engineering*, vol. 148, pp. 53–73.
- Freeman, E.; Weiland, L. M.** (2009): High energy density nastic materials: parameters for tailoring active response. *Journal of Intelligent Material Systems and Structures*, vol. 20, no. 2, pp. 233–243.
- He, X.; Ren, L.** (2005): Finite volume multiscale finite element method for solving the groundwater flow problems in heterogeneous porous media. *Water Resources Research*, vol. 41, W10417 doi:10.1029/2004WR003934.
- Hou, T. Y.** (2005): Multiscale modelling and computation of fluid flow. *International Journal for Numerical Methods in Fluids*, vol. 47, pp. 707–719.
- Hou, T. Y.; Wu, X. H.** (1997): A multiscale finite element method for elliptic problems in composite materials and porous media. *Journal of Computational Physics*, vol. 134, pp. 169–89.
- Hou, T. Y.; Wu, X. H.; Cai, Z. Q.** (1999): Convergence of a multiscale finite element method for elliptic problems with rapidly oscillating coefficients. *Mathematics of Computation*, vol. 68, pp. 913–943.
- Jenny, P.; Lee, S. H.; Tchelepi, H. A.** (2003): Multi-scale finite volume method for elliptic problems in subsurface flow simulation. *Journal of Computational Physics*, vol. 187, pp. 47–67.
- Kanoute, P.; Boso, D. P.; Chaboche, J. L.; Schrefler, B. A.** (2009): Multiscale methods for composites: a review. *Archives of Computational Methods in Engineering*, vol. 16, pp. 31–75.

Ken-ichiro, M.; Kozo, O.; Masanori, S. (1991): Finite element modelling of forming process of solid metal with liquid phase. *Journal of Materials Processing Technology*, 27, pp. 111-118.

Markovic, D.; Ibrahimbegovic, A. (2004): On micro–macro interface conditions for micro-scale based FEM for inelastic behavior of heterogeneous materials. *Computer Methods in Applied Mechanics and Engineering*, vol. 193, pp. 5503–5523.

Miehe, C.; Bayreuther, C. G. (2007): On multiscale FE analyses of heterogeneous structures: From homogenization to multigrid solvers. *International Journal for Numerical Methods in Engineering*, vol. 71, pp. 1135–1180.

Okada, H.; Fukui, Y.; Kumazawa, N. (2004): Homogenization Analysis for Particulate Composite Materials using the Boundary Element Method. *CMES: Computer modeling in engineering & sciences*, vol. 5, no. 2, pp. 135–150.

Paumelle, P.; Hassim, F.; Lene, F. (1991): Microstress analysis in woven composite structures. *Recherche Aerospaciale*, vol. 6, pp. 47–62.

Piyasena, M. E.; Newby, R.; Miller, T. J.; Shapiro, B.; Smela, E. (2009): Electroosmotically driven microfluidic actuators. *Sensors and Actuators B: Chemical*. vol. 141, pp. 263–269.

Schrefler, B. A. (2005): Multiscale modelling. In: Zienkiewicz OC, Taylor RL (eds) *The Finite Element Method for Solid and Structural Mechanics*. Elsevier, Amsterdam.

Sundaresan, V. B.; Leo, D. J. (2005): Chemo-mechanical Model of Biological Membranes for Actuation Mechanisms. *Proceedings of SPIE, Smart Structures and Materials: Active Materials: Behavior and Mechanics*, San Diego, CA, 2005, vol. 5761, pp. 108–118.

Suquet, P. (1987): Elements of homogenization theory for inelastic solid mechanics, In: Sanchez-Palencia, E., Zaoui, A. (Eds.), *Homogenization Techniques for Composite Media*. Springer-Verlag, Berlin, pp. 194–275.

Terada, K.; Kikuchi, N. (2001): A class of general algorithms for multi-scale analyses of heterogeneous media. *Computer Methods in Applied Mechanics and Engineering*, vol. 190, pp. 5427–5464.

Wang, H.T.; Yao, Z.H. (2005): A new fast multipole boundary element method for large scale analysis of mechanical properties in 3D particle-reinforced composites, *CMES: Computer Modeling in Engineering & Sciences*, vol. 7, no. 1, pp. 85–95.

Yang, Q. S.; Becker, W. (2004): A comparative investigation of different homogenization methods for prediction of the macroscopic properties of composites. *CMES: Computer modeling in engineering & sciences*, vol. 6, no. 4, pp. 319–332.

Yuan, Z.; Fish, J. (2008): Toward realization of computational homogenization in

practice. *International Journal for Numerical Methods in Engineering*, vol. 73, no. 3, pp. 361–380.

Zhang, H. W.; Boso, D. P.; Schrefler, B. A. (2003): Homogeneous analysis of periodic assemblies of elastoplastic disks in contact, *International Journal for Multiscale Computational Engineering*, vol. 1, no. 4, pp. 349–370.

Zhang, H. W.; Fu, Z. D.; Wu, J. K. (2009): Coupling multiscale finite element method for consolidation analysis of heterogeneous saturated porous media. *Advances in Water Resources*, vol. 32, pp. 268–279.

Zhang, H. W.; Wu, J. K.; Fu, Z. D. (2009): Extended multiscale finite element method for mechanical analysis of periodic lattice truss materials. *International Journal for Multiscale Computational Engineering*, Accepted and to be published.

Zhang, H. W.; Wu, J. K.; Fu, Z. D. (2010): Extended multiscale finite element method for elasto-plastic analysis of 2D periodic lattice truss materials. *Computational Mechanics*, vol. 45, pp. 623–635.

Zhang, H. W., Wu, J. K.; Liu, H.; Fu Z. D. (2010): Basic theories of extended multiscale finite element method. *Computer Aided Engineering*, vol. 19, pp. 3–9.

Zhang, H. W.; Wu, J. K.; Lv, J.; Fu, Z. D. (2010): Extended Multiscale Finite Element Method for Mechanical Analysis of Heterogeneous Materials. *Acta Mechanica Sinica*, doi 10.1007/s10409-010-0393-9.

